Effects of Au Plating on Dynamic Resistance during Small-Scale Resistance Spot Welding of Thin Ni Sheets

W. TAN, S. LAWSON, and Y. ZHOU

The effects of Au plating on dynamic resistance during small-scale resistance spot welding of thin Ni sheets have been investigated. Compared to the small-scale resistance spot welding of bare Ni, the Au-plated material showed much lower initial static resistance, and the contribution of constriction resistance to overall dynamic resistance reduced to a negligible value very early in the welding sequence because of the low softening temperature and its lack of surface oxide film. For the same reason, the asperity heating and surface breakdown stages during resistance spot welding of bare Ni were not observed during resistance spot welding of Au-plated Ni. Furthermore, the partial surface melting stage was replaced by the solid-state bonding and brazing stages. Step increases in the sheet-to-sheet dynamic resistance curves of Au-plated Ni were shown to be due to the peripheral unzipping of a prior solid-state bond caused by uneven local thermal expansion. The electrode-to-electrode dynamic resistance curve when welding Au-plated material is not useful for monitoring the state of nugget formation.

I. INTRODUCTION

IN resistance spot welding (RSW), the heat to form a weld is generated by the resistance to the flow of electric current through the sheets being joined. This resistance involves electrode and sheet bulk resistances as well as electrode-to-sheet and sheet-to-sheet contact resistances.[1] Study of the changes in resistance during welding (dynamic resistance) can help in understanding process mechanisms,[2] optimizing process parameters,[3] and developing quality control strategies.[4] Therefore, dynamic resistance behavior during RSW has attracted much research interest.

Up to the present time, most detailed process studies of RSW have been concerned with "large scale" resistance spot welding (LSRSW) of relatively thick sheet steels (thicker than 0.6 to 0.8 mm) mainly for applications in the automotive and appliance industries.[5,6] For fabrication of electronic and medical devices, a small-scale version of RSW (SSRSW) is being increasingly used, requiring much more precise electrical and mechanical control, lower electrode force, and current/energy input. There is currently very little available information about fundamental process characteristics of SSRSW, including dynamic resistance behavior, and the present work is part of a series of investigations aimed at satisfying that demand.

In a previous study,[7] weld nugget development has been characterized in SSRSW of 0.2-mm-thick Ni sheet. Both bare and gold-coated materials were welded, and large differences were found in the response of these materials related to differences in the physical/chemical nature of their surfaces. While the Au-coated sheet displayed solid-state bonding and brazing prior to the commencement of melting of Ni, the bare Ni sheet showed no bonding until base metal melting began. The dynamic resistance behavior during welding of bare Ni sheets has been characterized,[8] and clear indications have been seen of oxide film breakdown and persistence of constriction resistance effects up to the beginning of melting. In the present work, the relationship between nugget development and dynamic resistance curves has been studied during SSRSW of Au-plated Ni, and the results are compared to those of welding on bare Ni.

W. TAN, formerly Graduate Student, Microjoining Laboratory, Department of Mechanical Engineering, University of Waterloo, is Research Associate, University of Wisconsin–Madison, Madison, WI 53706. S. LAWSON, Adjunct Professor, and Y. ZHOU, Associate Professor, are with the Microjoining Laboratory, Department of Mechanical Engineering, University of Waterloo, Waterloo, ON, Canada N2L 3F1.

Manuscript submitted August 26, 2004.

II. TECHNICAL BACKGROUND

Contact resistance is a useful theoretical idealization of the real physical situation. For example, in experiments (Figure 1), the measured sheet-to-sheet resistances always include part of the sheets' bulk resistance.[6] Therefore, the dynamic resistance, R, between two sheets will follow the equation:

$$R = R_C + R_B \quad [1]$$

where R_C and R_B are the constriction resistance and bulk resistance, respectively.

When sheet-to-sheet dynamic resistance is measured, as shown in Figure 1, the bulk resistance contribution R_B involves an effective path length l of one sheet thickness and can be calculated using the following equation:

$$R_B = \rho \frac{l}{A} \quad [2]$$

where ρ is the resistivity and A is the effective area of current path.

For metals with clean surfaces, the contact resistance is equal to the constriction resistance.[9,10] The constriction resistance R_C has frequently been found to follow the relationship[9]

$$R_C = 0.89\,\rho\left(\frac{\xi H}{nF}\right)^{\frac{1}{2}} \quad [3]$$

where ρ is the resistivity of contact spots, H is the hardness, F is the compressive force, ξ is the pressure factor, its value ranging from about $\xi = 0.2$ for surfaces with considerable elastic action to $\xi = 1.0$ for totally plastic contact. A value of

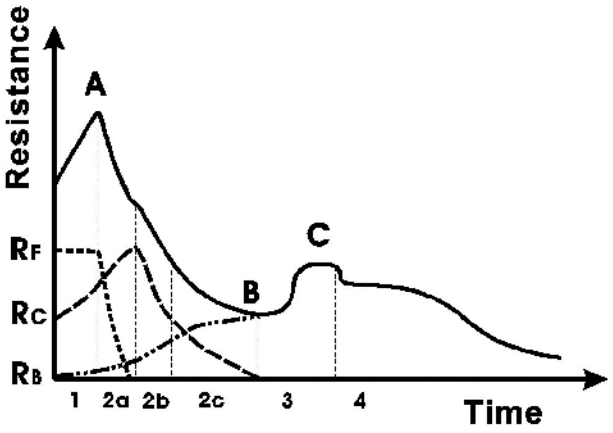

Fig. 1—Schematic showing a typical dynamic resistance curve during SSRSW of Ni.[8]

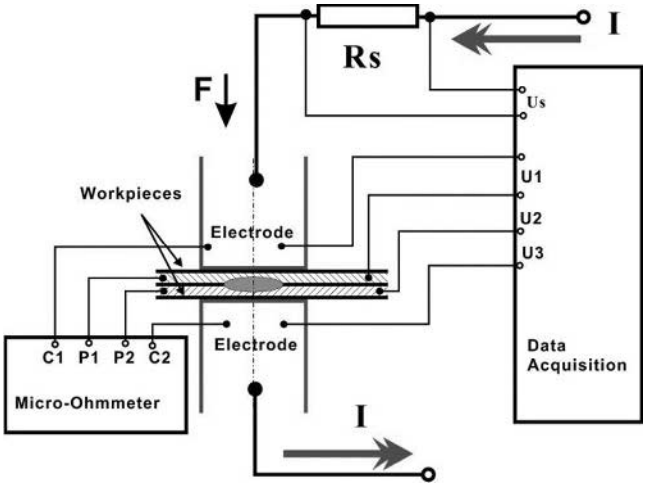

Fig. 2—Experimental setup.

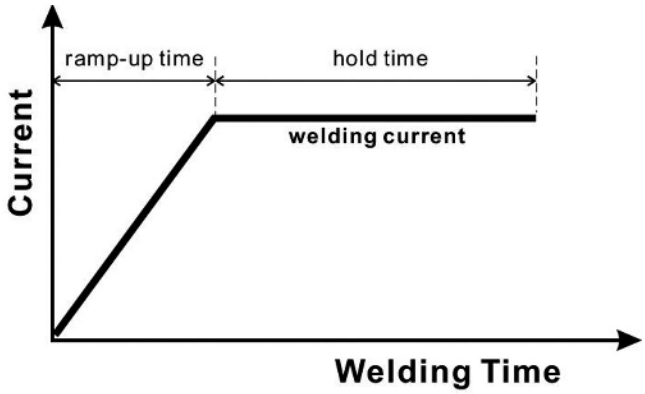

Fig. 3—Current waveform.

$\xi = 0.7$ is often a fair approximation when detailed study is not warranted.[10] The term n is the contact spot number; polished, well-rounded crossed cylinders tend toward $n = 1$, while large, overlapping, flat, electroplated surfaces have values of n more often between 10 and 20.[10] When surfaces have reaction or other films, *e.g.*, due to surface oxidation, an additional film resistance term appears in the total measured contact resistance, as found for instance in welding of bare nickel sheets.[8]

From Eq. [1], the dynamic resistance during RSW is the result of the sum of bulk resistance and constriction resistances, and the dominance of each component may change during the welding sequence. For example, the passage of welding current would increase the bulk resistance by increasing temperature and hence the resistivity but might reduce the constriction resistance by enlarging the contact spots.

It has been shown that the only bonding mechanism for SSRSW of bare Ni is fusion bonding, and the bonding mechanisms for SSRSW of Au-plated Ni include solid-state bonding, brazing, and fusion nugget formation.[7] Based on the physical changes at the faying surface, the dynamic resistance curve for SSRSW of bare Ni has been defined as including the following stages (Figure 1): (1) asperity heating, (2a) surface breakdown, (2b) asperity softening, (2c) partial surface melting, (3) nugget growth, and (4) expulsion.[8] Since the interaction and bonding phenomena seen in welding Au-plated Ni are quite different from those of bare Ni, the dynamic resistance behavior in welding of the Au-plated material is expected to be correspondingly different from that for bare Ni.

III. EXPERIMENTAL PROCEDURE

The Au-plated Ni sheets (Ni 200, annealed) 0.2 mm in thickness were used in this study. The thickness of the Au plating layer was about 4 μm, with a root-mean-square roughness of 380 nm. Lap-welded joints were made using coupons approximately 40-mm long and 8-mm wide, with the two sheets placed such that their rolling directions were parallel. Prior to welding, the samples were ultrasonically cleaned for 10 minutes in acetone.

A DC welding power supply MacGregor DC4000P (MacGregor Welding Systems Ltd., Mildenhall, Suffolk, UK) was applied in this study. The weld head was Unitek 80A/115 (air activated) (Miyachi Unitek Corp., Monrovia, CA). Flatended round RWMA class 2 (Cu-Cr) electrodes 3.2 mm in diameter were used. The experimental setup is shown in Figure 2. The initial static resistance was measured using a digital microohmmeter after welding force was applied but before the welding current was initiated. Dynamic signals were monitored by a data acquisition system controlled by a PC running MATLAB. A standard resistor R_s was in series in the welding current loop; the voltage drop through the resistor U_S was recorded by the data acquisition system. The welding current was computed as $I = U_S/R_s$. The voltage drops through the electrode-to-sheet and sheet-to-sheet interfaces were recorded as U_1, U_3, and U_2. The dynamic resistances through the three interfaces were calculated as $R_1 = U_1/I$, $R_2 = U_2/I$, and $R_3 = U_3/I$, respectively. Welding current was programmed as shown in Figure 3 with a ramp-up time of 30 ms and variable hold times. The welding force was 51 N. As-welded joints were peeled and the bond area diameters were estimated from the fractured faying surfaces or pulled-out buttons using a scanning electron microscope (SEM).

IV. RESULTS

In Figure 4(a), typical sheet-to-sheet dynamic resistance curves are shown for nominal welding currents of 2500,

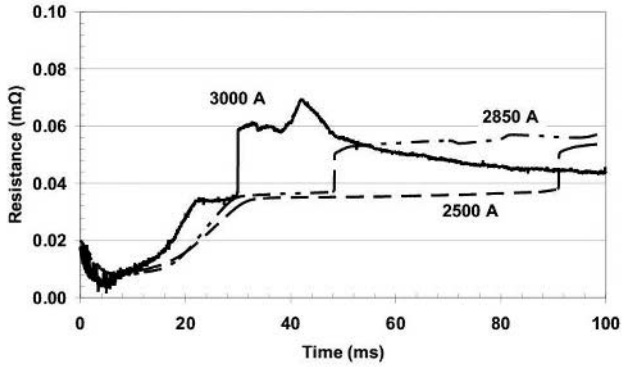

(*a*)

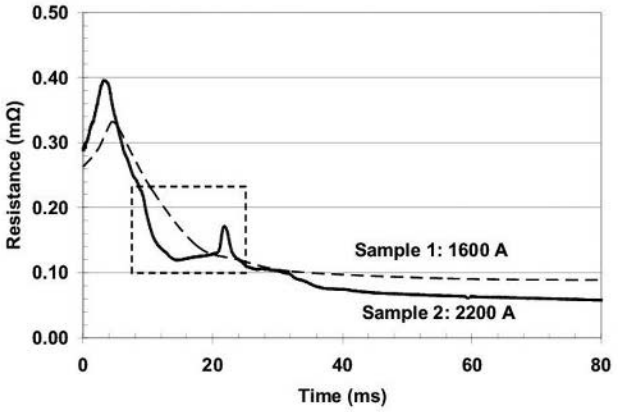

(*b*)

Fig. 4—(*a*) Sheet-to-sheet dynamic resistances for Au-plated Ni and (*b*) sheet-to-sheet dynamic resistances for bare Ni[8] with different welding currents.

2850, and 3000 with 99-ms hold time. With 2500-A welding current, a solid-state bonded joint was produced. At 2850-A welding current, a brazed joint was produced. When the welding current reached 3000 A, a fusion nugget formed at the faying surface.

In Figure 4(b), typical corresponding dynamic resistance curves from Reference 8 are shown for SSRSW of bare Ni sheets, for welding current at 1600 A giving a partial surface melting joint and at 2200 A giving a fusion nugget joint. The extremely different response of these two materials may immediately be noticed, with the bare Ni behavior initially dominated by film resistance and showing a very slow rate of contact resistance decrease after film breakdown.

To further investigate the relationship between dynamic resistance and nugget formation, a group of joints was made with 3000-A welding current, but the welding process sequences were terminated at different instants. The initial sheet-to-sheet static resistances were, based on 12 samples, about 0.015 ± 0.004 mΩ (the mean plus or minus one standard deviation). The dynamic resistance results are shown in Figures 5 through 10 and are described subsequently.

When the welding current was shut down at 5 ms, the sheet-to-sheet dynamic resistance was found to have decreased continuously (Figure 5(a)). The SEM examination indicated that the asperities at the faying surface were greatly flattened (indicated by the arrows in Figure 5(b)) compared with the faying surface before the application of welding current

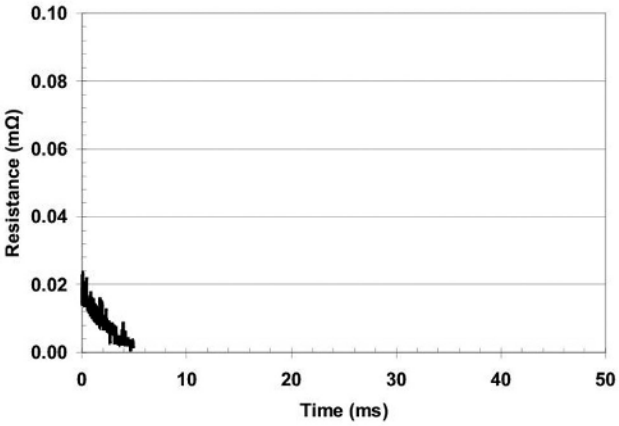

(*a*)

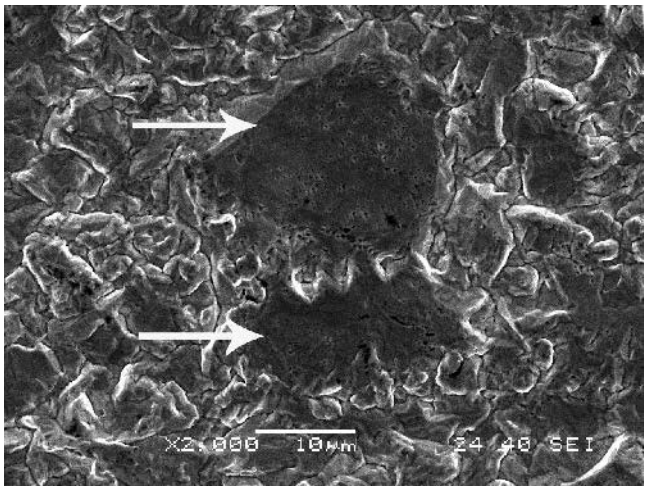

(*b*)

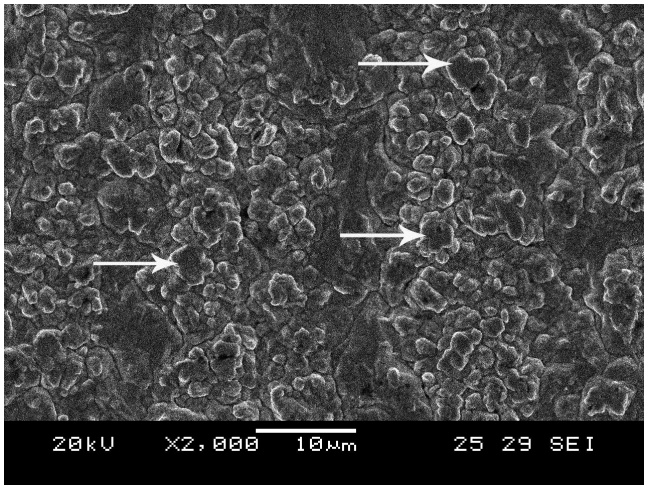

(*c*)

Fig. 5—(*a*) Sheet-to-sheet dynamic resistance curve and (*b*) faying surface for sample made at 5 ms as well as (*c*) faying surface before the application of welding current.

(Figure 5(c)), in which some plastic deformation of contacting asperities (indicated by the arrows) was found under the electrode force. No evidence of bonding was seen on the

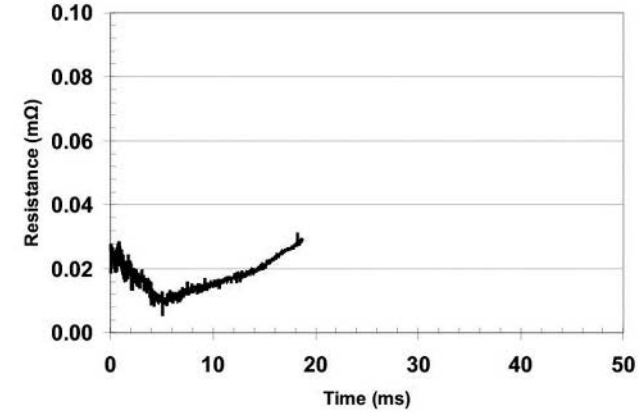

(*a*)

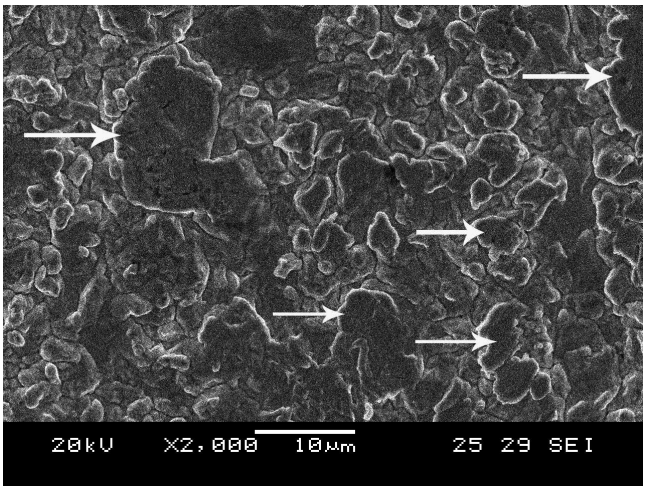

(*b*)

Fig. 6—(*a*) Sheet-to-sheet dynamic resistance curve and (*b*) faying surface for sample made at 26 ms.

separated faying surfaces by this instant. The decrease in dynamic resistance at this stage is consistent with the increasing area of contacting asperities and is believed to be caused by heating and softening of the asperities.

When the welding current was shut down at 19 ms, the sheet-to-sheet dynamic resistance was found to have decreased for only the first 5 ms, then a monotonic increase was seen (Figure 6(a)). Faying surface examination showed greatly flattened asperities (indicated by the arrows in Figure 6(b)); however, no bonding had yet occurred. The increase in dynamic resistance was tentatively attributed to increased bulk resistivity caused by heating of the joint assembly.

When the welding current was shut down at 28 ms, the sheet-to-sheet dynamic resistance reached a plateau (Figure 7(a)) at about 21 ms. The SEM examination indicated that some solid-state bonding[7] had occurred at the faying surface (Figures 7(b) and (c)), which failed by ductile failure on testing, as shown in Figure 7(c).

When the welding current was shut down at 29 ms, the sheet-to-sheet dynamic resistance was still at the same plateau (Figure 8(a)), but a brazing area[7] with 0.6-mm diameter had formed at the faying surface (Figure 8(b)).

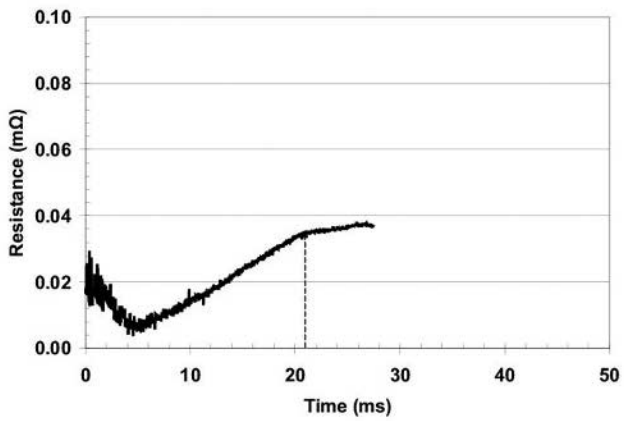

(*a*)

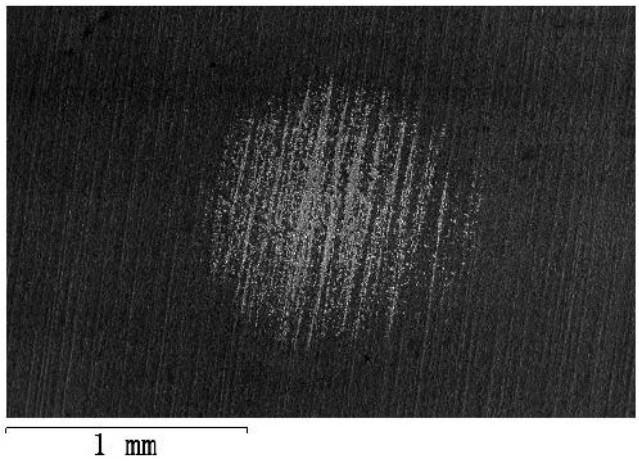

(*b*)

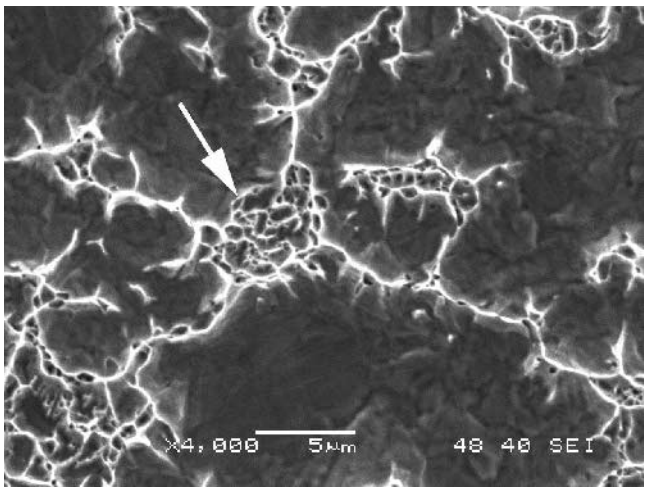

(*c*)

Fig. 7—(*a*) Sheet-to-sheet dynamic resistance curve and (*b*) low-magnification faying surface as well as (*c*) high-magnification faying surface of sample made at 28 ms.

When the welding current was shut down at 37 ms, the sheet-to-sheet dynamic resistance curve showed a step increase at about 31 ms (Figure 9(a)). Subsequent to the step increase, small ripples occurred in the sheet-to-sheet dynamic

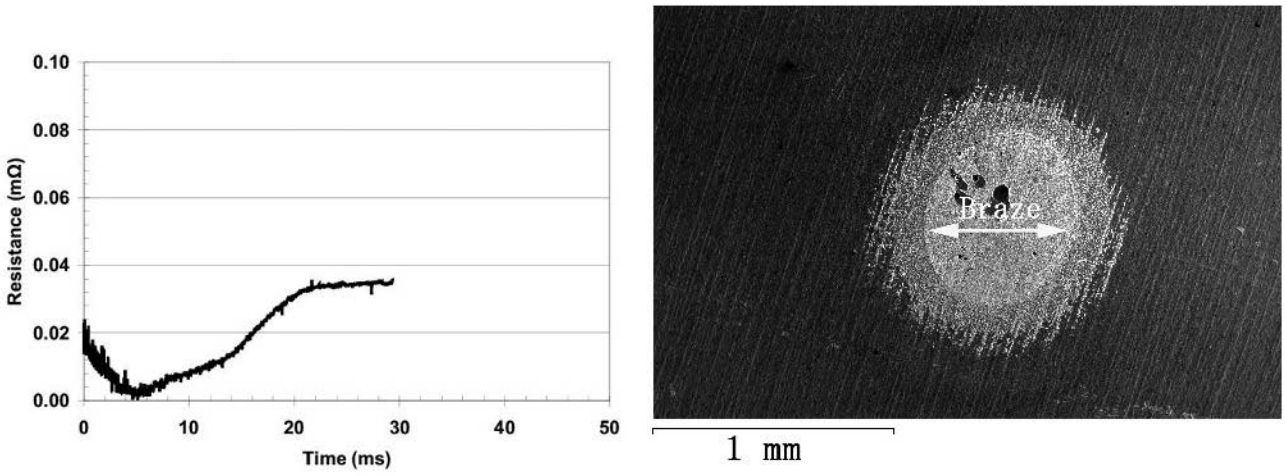

(*a*) (*b*)

Fig. 8—(*a*) Sheet-to-sheet dynamic resistance curve and (*b*) fractured faying surface of sample made at 29 ms.

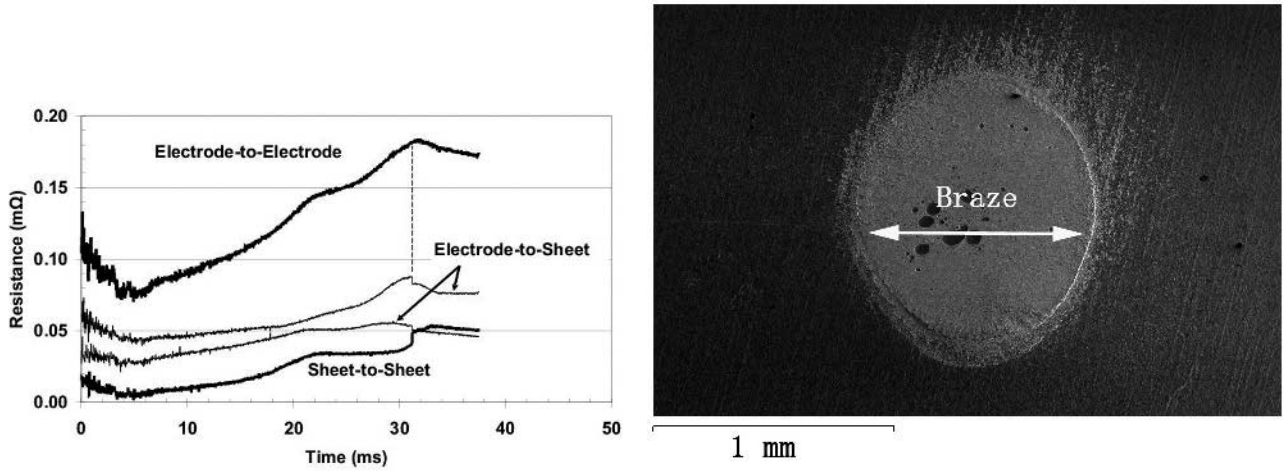

(*a*) (*b*)

Fig. 9—(*a*) Dynamic resistance curves and (*b*) fractured faying surface of sample made at 37 ms.

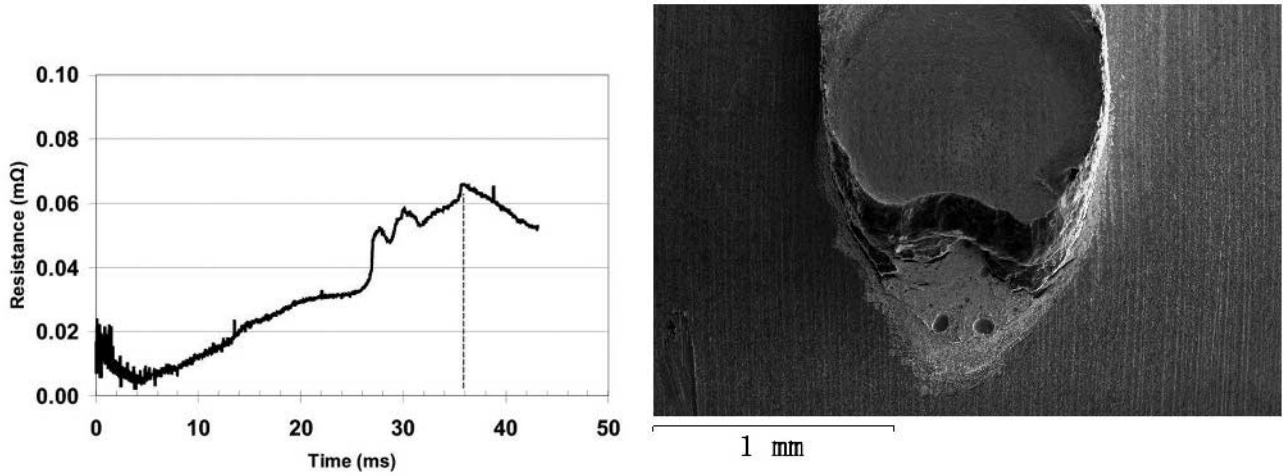

(*a*) (*b*)

Fig. 10—(*a*) Sheet-to-sheet dynamic resistance curve and (*b*) fractured faying surface of sample made at 43 ms.

Table I. Material Properties[10]

Element	Softening Temperature (°C)	Melting Temperature (°C)	Room-Temperature Resistivity (10^{-7} Ωm)	Hardness (10^8 N/m^2)	Elastic Modulus (10^8 N/m^2)
Ni	520	1455	0.684	6.9	1960
Au	100 to 200[12]	1064	0.218	2.5	800
Fe	500	1535	0.97	5.9	1960

resistance curve. The SEM examination indicated that a brazing area with 1.0-mm diameter was formed at the faying surface (Figure 9(b)). The examination of other dynamic resistance curves showed that at the same instant, there were corresponding step reductions in the electrode-to-sheet dynamic resistance curves (Figure 9(a)), while the electrode-to-electrode dynamic resistance showed smooth change. These features of the dynamic resistance behavior are discussed in Section V.

When the welding current was shut down at 43 ms, the sheet-to-sheet dynamic resistance showed a small peak after the ripple area (at about 36 ms in Figure 10(a)). A pulled-out button was produced after the peel test (Figure 10(b)). A fusion nugget[7] in 0.8-mm diameter was seen to be formed at the faying interface after cross sectioning this sample. The small peak at the sheet-to-sheet dynamic resistance curve is believed to be due to the formation of fusion nugget, as discussed subsequently.

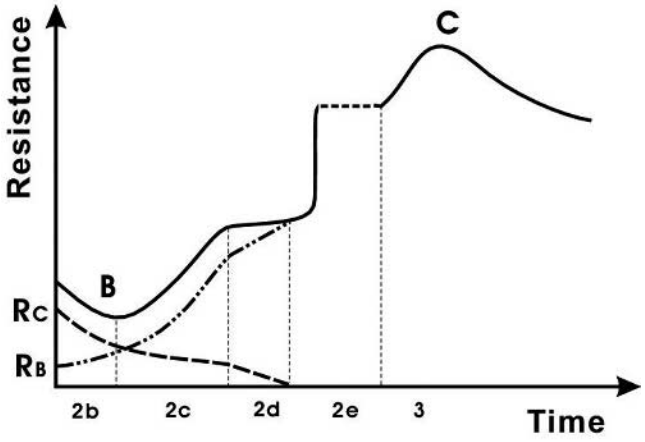

Fig. 11—Schematic showing a typical dynamic resistance curve at the faying surface during SSRSW of Au-plated Ni.

V. DISCUSSION

A. *Initial Static Resistance*

At room temperature, the resistivity of Au is 0.218×10^{-7} Ωm. The hardness of thin Au electroplate at room temperature is taken as 2.5×10^8 N/m^2.[10] Equation [3] predicts a constriction resistance for the Au surface at room temperature of 0.0087 to 0.0123 mΩ for the input data $\xi = 0.7$, $n = 10$ to 20,[10] $F = 51$ N, and $H = 2.5 \times 10^8$ N/m^2 as summarized in Table I. Since the thickness of the Au plating layer is so small (4 μm) compared with the thickness of the Ni sheets (0.2 mm), and the resistivity of Au is less than 1/3 of that of Ni (Table I), the contribution to bulk resistance of the Au plating layer will be insignificant. Because of the small thickness and because the Au elastic modulus is much smaller than that of Ni (Table I, 800×10^8 N/m^2 for Au *vs* 1960×10^8 N/m^2 for Ni and Fe), the elastic response and hence the apparent contact diameter of the Au-plated sheets at the faying surface should be essentially similar to that of bare Ni and Fe sheets, *i.e.*, 4.8 mm based on the model of Chang.[11] At room temperature, the resistivity of Ni is 0.684×10^{-7} Ωm; therefore, the contribution of bulk resistance at room temperature would be about 0.0008 mΩ by Eq. [2] with $l = 0.2$ mm. The total predicted sheet-to-sheet resistance by Eq. [1] is therefore 0.0095 to 0.0131 mΩ, which is very close to the measured sheet-to-sheet initial static resistance (0.011 to 0.019 mΩ).

B. *Dynamic Resistance*

Comparison of Figures 4(a) with (b) shows that the presence of gold plating on the Ni surface caused a major reduction in the initial static resistance of the loaded joint assembly, and also major changes in the dynamic evolution of joint resistance during welding. In comparison with the bare Ni case,[8] the welding sequence could also be broken down into stages; however, some new stages were clearly evident, while some stages found to be important in welding of bare Ni were absent in the present work. For consistency with the numbering system developed to describe the bare Ni welds, the following stages of development of dynamic resistance R have been defined for Au-plated Ni (Figure 11): 2b, asperity softening; 2d, temperature increase; 2e, solid-state bonding; 2f, brazing; and 3, nugget growth. The relative contributions to dynamic resistance of dynamic constriction resistance R_C and bulk R_B during a welding sequence are illustrated schematically in Figure 11, which also shows the process stages and time instants defined previously.

While the Au plating caused major changes in the shapes of dynamic resistance curves, those shapes are still determined essentially by two competing processes. The electric power dissipated in the joint assembly causes heating with a corresponding increase in resistivity of bulk material and asperities, tending to increase dynamic resistance with time. However, the heating also leads to softening of asperities tending to increase electrical contact area, reducing constriction resistance and overall dynamic resistance. The impact of these effects in the successive stages of the welding process is discussed in Sections 1 through 5.

1. *Stage 2b*

As shown in Figures 5(a), 6(a), 7(a), 8(a), 9(a), and 10(a), the sheet-to-sheet dynamic resistance showed a sharp and significant reduction starting immediately on application of welding current and continuing for about 5 ms. As described

in Section II-B, constriction resistance would be a dominant component of the total contact resistance at the commencement of welding, and that in turn is strongly related to surface hardness. As faying surface heating begins due to the passage of welding current, hardness will decrease, with the most significant reduction occurring around the recrystallization temperature. Hardness decrease will lead in turn to decrease in constriction resistance, in accordance with Eq. 3. The recrystallization temperature of thin pure gold films is quite low, ~100 °C to 200 °C,[12] and therefore softening should begin nearly immediately upon application of welding current. This is consistent with the observation of immediate reduction of constriction resistance, and with the metallographic evidence of significant growth in the deformed area of surface asperities after 5 ms (Figure 5(b) *vs* 5(c)).

2. *Stage 2d*

As shown in Figure 12, the resistivities of Au and Ni increase as temperature increases. The result is an increase in the contribution of bulk resistance to the total dynamic resistance. For instance, by 900 °C bulk temperature, which is well below the minimum melting point of Ni-Au alloy (no less than 955 °C[13]), the resistivity of Ni is 5.1×10^{-7} Ωm (Figure 12 and Table II), and if the diameter of the current-carrying path is assumed to be 2.5 mm,[11] the sheet-to-sheet bulk resistance could be about 0.021 mΩ by Eq. [2], which is much higher than the predicted room-temperature constriction resistance (0.0087 to 0.0123 mΩ). Considering the constriction resistance decreases with the flattening of asperities, as the sheets heat in the range 200 °C to 900 °C, bulk resistance should gradually replace constriction resistance as the dominant component of the total dynamic resistance, and the measured resistance should increase with temperature, as seen in Figures 6 through 10.

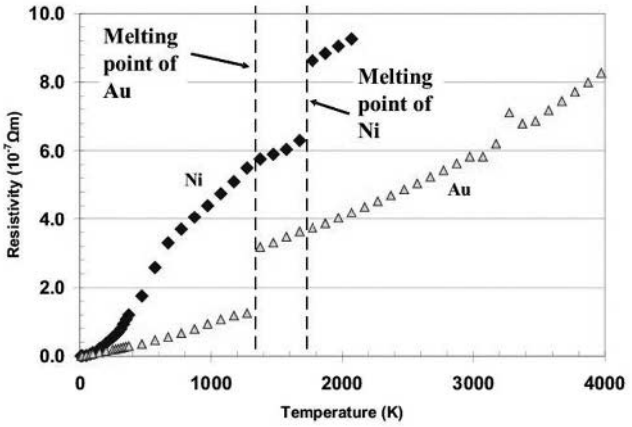

Fig. 12—Resistivity *vs* temperature for pure Ni and Au.

Table II. Resistivity of Ni and Au at Different Temperatures[16]

Temperature (°C)		20	200	900	1000	1400	1500
Resistivity (10^{-7} Ωm)	Ni	0.684	1.75	5.1	5.5	6.3	8.63
	Au	0.218	0.347	1.18	1.25	3.63	3.74

3. *Stage 2e*

The Au does not oxidize in air. Moreover, thermal desorption of adsorbed surface contaminants is commonly seen on Au surfaces when heated.[14] This effect together with thermal softening should make it easier for more of the faying surfaces to be easily brought into atomic contact by electrode force, as the joint assembly is heated. Metallographic and dynamic resistance evidence confirmed that, as welding progressed, the contact spots continuously merged and the constriction resistance gradually disappeared, so that the dynamic resistance finally consisted of only bulk resistance by the end of the solid-state bonding stage. Final elimination of constriction resistance, and some continued growth in the effective diameter of contact would offset the increase of bulk resistance; therefore the sheet-to-sheet dynamic resistance appears to plateau at this stage. Before melting occurs, the contact diameter at the faying surface decreases as temperature increases due to uneven thermal expansion.[11] Therefore, at the end of the solid-state bonding stage, at which the temperature is very close to the brazing temperature (955 °C[13]), the contact diameter should be smaller than 2.5 mm, and the sheet-to-sheet bulk resistance should be larger than the 0.021 mΩ value calculated earlier. The observed height of the plateau is found to be about 0.035 mΩ (Figures 7 through 10) and confirms this justification.

4. *Stage 2f*

As temperature increased, melting would start at the Ni-Au interface thanks to the lower melting point of Ni-Au alloy compared with the pure Ni and Au.[13] When the Au plating layer was consumed, brazing occurred.[7] During the braze development, a sudden step increase was seen in the sheet-to-sheet dynamic resistance curve, and at the same instant, a step decrease appeared at the electrode-to-sheet dynamic resistance curves (Figure 9(a)). The formation of the steps will be discussed in Part D of Section V. Pores were produced and then squeezed away from the center of the brazing area.[7] The small ripples after the step may be related to the generation and movement of porosity. The small ripples were not found during SSRSW of bare Ni since no porosity was generated in the welding process.

5. *Stage 3*

It has been shown that there is large resistivity difference between liquid Ni phase and solid Ni (Figure 12), so as the fusion nugget forms and grows, the dynamic resistance would be expected to correspondingly increase until the nugget reaches its maximum diameter or thickness at the *C* instant. Correlation of dynamic resistance and metallographic data showed that, at the *C* peak, the nugget was almost at its maximum at diameter of 0.8 mm, according to the cross sections of samples made at 3000 A. If the central portion of the joint is assumed to be a liquid cylinder of 0.8-mm diameter and 0.2-mm length, the bulk resistance of the nugget would be about 0.344 mΩ by Eq. [2] using a liquid Ni resistivity value at 8.63×10^{-7} Ωm (Table II). The fused material is surrounded by the brazing and solid-state bonding areas, and the outer diameter of the contact area at this stage is estimated to be about 1.5 mm (Figure 10(b)); the bulk resistance of the surrounding solid nickel is about 0.100 mΩ by Eq. [2] using a resistivity value of 6.3×10^{-7} Ωm (Table II). These two bulk resistances are parallel and the equivalent sheet-to-sheet bulk resistance is about 0.077 mΩ, which is very close to the observed peak value in Figure 10(a) (0.066 mΩ).

C. *Effects of Au Plating*

In SSRSW of bare Ni sheets, the evolution of dynamic resistance during welding was shown to be incipiently dominated by the presence of surface oxide films.[8] The voltage required to cause film breakdown implied a high initial value of dynamic resistance, and the persistence of the film plus relatively higher softening temperature of Ni than that of Au (Table I) led to very slow growth of the contact area with increasing faying surface temperature, causing constriction resistance to continue as a dominant contributor to total dynamic resistance until the beginning of melting, as shown in Figure 1.

Comparison of Figures 4(a) with (b) shows that the presence of the gold plating on the Ni surface caused a major reduction in the initial static resistance of the loaded joint assembly, and also major changes in the dynamic evolution of joint resistance during welding. In comparison with the bare Ni case,[8] some new stages were clearly evident, while some stages found to be important in welding of bare Ni were absent during SSRSW of Au-plated Ni. The stage evolution is summarized as Table III.

Compared with the bare Ni case, stage 1, the initial dynamic resistance increase due to asperity heating prior to oxide film breakdown does not occur during SSRSW of Au-plated Ni due to rapid softening of Au plating and contact area growth. Stage 2a, film breakdown, does not occur with Au-plated sheets due to the absence of oxide film. Stage 2b appeared in both cases because both bare Ni sheets and Au-plated sheets are contacted at asperities under compressive force, and their constriction resistances made similar important contributions to the sheet-to-sheet dynamic resistance before the bulk temperature rose.

Prior to any melting, both bare Ni sheets and Au-plated Ni sheets experience bulk temperature increases. However, for the bare Ni case, the resultant bulk resistance increase was not distinct in the dynamic resistance curve due to the slow growth of contact area with increasing faying surface temperature, causing constriction resistance to continue as a dominant contributor to sheet-to-sheet dynamic resistance until the beginning of melting. For the Au-plated Ni, the initial constriction resistance (0.0087 to 0.0123 mΩ) was much lower than that of bare Ni (0.04 to 0.06 mΩ). On the other hand, the rapid softening of Au plating brought the constriction resistance down very early, so that the bulk resistance started to dominate the dynamic resistance before bonding occurred, and the temperature increase stage (2d) was introduced (Figure 11).

Table III. Comparison of the Stages between Bare Ni and Au-Plated Ni

Stage	Bare Ni	Au-Plated Ni
1. Asperity heating	√	
2a. Film breakdown	√	
2b. Asperity softening	√	√
2d. Temperature increase		√
2e. Solid-state bonding		√
2f. Brazing		√
2c. Partial surface melting	√	
3. Nugget growth	√	√
4. Expulsion	√	

For Au-plated Ni, the solid-state bonding (2e) and brazing (2f) stages were introduced due to the occurrence of new bonding mechanisms[7] caused by the Au plating. Stage 2c, the partial faying surface melting seen in bare Ni (Figure 1), is not seen here due to the prior occurrence of the solid-state bonding and Au-Ni brazing stages. Stage 3, nugget growth, is observed in both cases. Finally, stage 4, expulsion, cannot occur within the current limit of the power supply during welding of Au-plated Ni since the pressure of liquid nugget is much lower than that of bare Ni[7] and it remains sealed in a closed space by peripheral solid-state bonding. Other effects of Au plating on dynamic resistance are further discussed in Section D.

D. *Steps in Resistance Curves*

In Figures 9(a) and 10(a), the sudden upward step in dynamic resistance occurred during the brazing stage, and was initially assumed to be associated with the formation of braze liquid. Further welding experiments (Table IV) showed that at very low welding current, *e.g.*, 2300 A, the steps did not appear. With 2500 A welding current, the step occurred at about 91 ms (Figure 4a). With 2700 A welding current, the step occurred at about 60 ms (Figure 13). The joints made at 2500 and 2700 A were solid-state bonded. Therefore, it was suggested that the occurrence of steps requires a particular range of heat input/heating rate and was not necessarily related to the formation of braze liquid.

Chang's numerical modeling of SSRSW of mild steel[11] showed that the sheet-to-sheet contact diameter reduces from the 1.5 × electrode tip diameter to the 0.4 × electrode tip diameter during the first two cycles due to uneven thermal expansion of the workpiece, as illustrated schematically in Figure 14. A comparable local thermal expansion will also

Table IV. The Resistance Steps at Different Currents

2300 A	2500 A	2700 A	2850 A	3000 A
Solid-state bonding, no step	Solid-state bonding, step at 91 ms (Fig. 4(a))	Solid-state bonding, step at 60 ms (Fig. 13)	Brazing, step at 48 ms (Fig. 4(a))	Fusion nugget, step at 30 ms (Fig. 4(a))

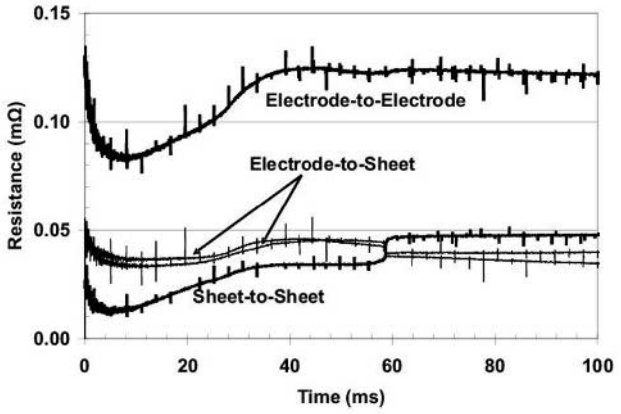

Fig. 13—Dynamic resistance curves of sample made at 2700 A.

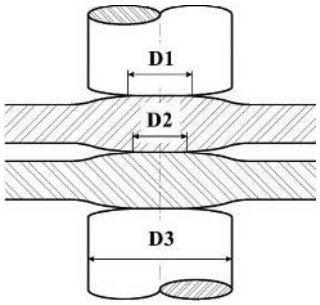

Fig. 14—Schematic of contact during SSRSW.

occur during SSRSW of Au-plated Ni, and the reduction of sheet-to-sheet contact radius is expected. If local heating and expansion of a column of material between the electrodes causes the peripheral region of the contact area to no longer carry compressive welding force, and if that region is solid-state bonded, the reduction of electrical contact radius could be temporarily arrested causing a tensile stress concentration at the outer edge of the bonding area. When the concentrated tensile stress exceeds the local bond strength, it will cause the unzipping of the solid-state bonding area with reduction of the effective current carrying diameter and corresponding increase in dynamic resistance. The resultant redistribution of the sheet stress could also cause an increase in the diameter of electrode-to-sheet contact, with a corresponding step decrease in electrode-to-sheet dynamic resistance. In every case where a step increase was seen in sheet-to-sheet resistance, this was accompanied by step reduction in electrode-to-sheet resistance (Figures 9(a) and 13).

The SEM examination of faying sheet surfaces was carried out on weldment samples where resistance steps had occurred, after carefully peeling the coupons apart, and a typical result is shown in Figure 15. In all cases, bright, fresh ductile dimples in the center of the weld zone were surrounded by an annular zone around the periphery where dimples of a very dull appearance were seen. The difference in fracture surface morphology clearly suggests that these spots were peeled at different times. During welding, the bonded peripheral spots were peeled and fractured by the unzipping action described previously due to uneven thermal expansion. When the sample cooled, the weld zone tended to recover its original shape, causing the dimples formed by unzipping during welding to be deformed by the opposing peaks. This is evidently the cause of the difference in fracture appearance between the fracture surface peripheral and central zones.

E. *Control Issues*

During SSRSW of bare Ni, the shape of the electrode-to-electrode dynamic resistance curve was found to be very similar to the sheet-to-sheet dynamic resistance curve.[8] The electrode-to-electrode dynamic resistance curve during SSRSW of bare Ni indicates the state of nugget formation and could be used for quality control. However, during SSRSW of Au-plated Ni, the shape of the electrode-to-electrode dynamic resistance curves (Figure 16) was found to be different from the sheet-to-sheet dynamic resistance curves (Figure 4a). On the other hand, shapes of the electrode-

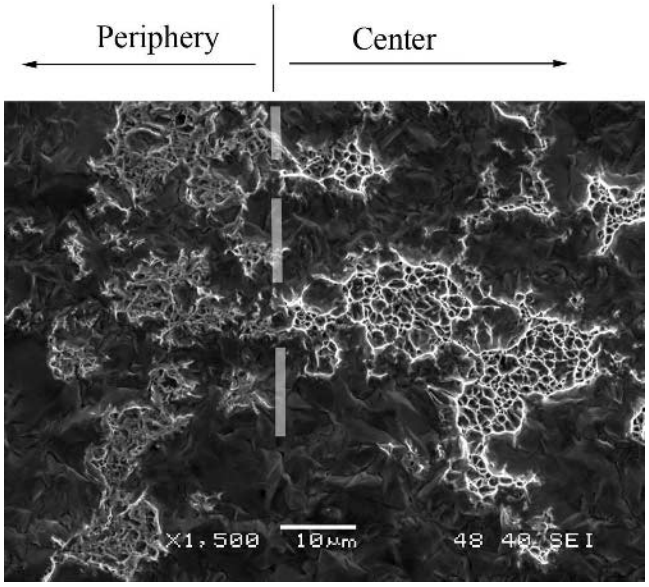

Fig. 15—Fractured faying surface of sample with which steps were showing at the dynamic resistance curves.

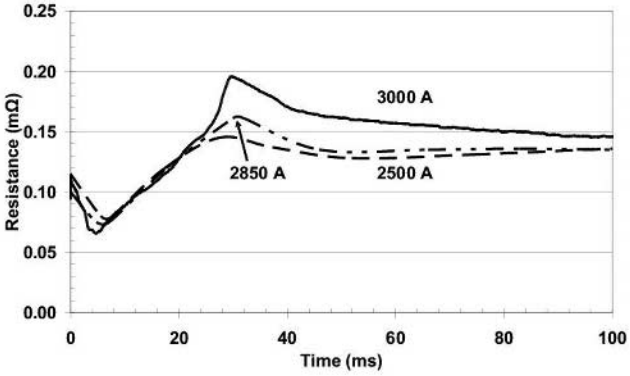

Fig. 16—Electrode-to-electrode dynamic resistance curves during SSRSW of Au-plated Ni at different currents.

to-electrode resistance curves for the situations of solid-state bonding, brazing, and fusion nugget are similar (Figure 16). Therefore, the electrode-to-electrode dynamic resistance curve for SSRSW of Au-plated Ni is much less useful for quality control since it does not indicate the state of nugget formation. This is consistent with the prior result of Gedeon and Eagar,[15] who showed that the electrode-to-electrode dynamic resistance curve during LSRSW of Zn-coated steel reflects the resistance change of the electrode-to-sheet interface as well as the resistance change of the sheet-to-sheet interface, making it difficult to use the electrode-to-electrode dynamic resistance as a quality control input variable.

VI. CONCLUSIONS

The effects of Au plating on the dynamic resistance during SSRSW of Ni have been investigated, coupled with postweld examination using tensile-shear testing, optical microscopy, scanning electron microscopy and energy-dispersive X-ray

spectroscopy. The major conclusions are summarized as follows.

1. Based on the physical changes at the faying surface, the sheet-to-sheet dynamic resistance curve for SSRSW of Au-plated Ni sheets can be defined in terms of the following stages: asperity softening, temperature increase, solid-stage bonding, brazing, and nugget growth.
2. Compared to the SSRSW behavior of bare Ni, the Au-coated material showed much lower initial static resistance, and the contribution of constriction resistance to overall dynamic resistance became relatively small much earlier in the welding sequence because of the low softening temperature of Au and its lack of surface oxide film. This resulted in a much more visible positive temperature effect on bulk resistivity and overall dynamic resistance for Au-plated material.
3. Step increases in the sheet-to-sheet dynamic resistance curves were due to the peripheral unzipping of a prior solid-state bond caused by uneven local thermal expansion.
4. The electrode-to-electrode dynamic resistance curve when welding Au-plated material is not useful for monitoring the state of nugget formation since the shapes of the electrode-to-electrode resistance curves for the situations of solid-state bonding, brazing, and fusion nugget are similar.

REFERENCES

1. *Resistance Welding Manual*, 5th ed., Resistance Welder Manufacturers' Association, Philadelphia, PA, 2003, pp. 1-3 to 1-4.
2. D.W. Dickinson, J.E. Franklin, and A. Stanya: *Welding Res. Suppl*., 1980, vol. 59 (6), pp. 170s-176s.
3. J.G. Kaiser, G.J. Dunn, and T.W. Eagar: *Welding Res. Suppl*., 1982, vol. 61 (6), pp. 167s-174s.
4. M. Towey and D.R. Andrews: *Welding Met. Fabr*., 1968, vol. 36 (10), pp. 383-92.
5. B.M. Brown: *Welding J*., 1987, vol. 66 (1), pp. 18-23.
6. W.F. Hess and R.L. Ringer: *Welding Res. Suppl*., 1938, vol. 17 (10), pp. 39s-48s.
7. W. Tan, Y. Zhou, and H.W. Kerr: *Metall. Mater. Trans. A*, 2002, vol. 33A, pp. 2667-75.
8. W. Tan, Y. Zhou, H.W. Kerr, and S. Lawson: *J. Phys. D, Appl. Phys*., 2004, vol. 37 (14), pp. 1998-2008.
9. *Electric Contacts Theory and Application*, R. Holm, ed., Springer-Verlag, New York, NY, 1967, pp. 9-26.
10. *Physical Design of Electronic System*, D. Baker *et al*., eds., Prentice-Hall Inc., Englewood Cliffs, NJ, 1971, vol. 3.
11. B.H. Chang, M.V. Li, and Y. Zhou: *Sci. Technol. Welding Joining*, 2001, vol. 6 (5), pp. 273-80.
12. *ASM Handbook* (formerly *Metals Handbook*, 10th ed.), ASM INTERNATIONAL, Materials Park, OH, 1992, vol. 2, pp. 704-05.
13. *Binary Alloy Phase Diagrams*, T.B. Massalski, ed., ASM Handbook, ibid., vol. 3, p. 273.
14. *Analytical Chemistry of the Noble Metals*, F.E. Beamish, Pergamon Press, Oxford, United Kingdom, 1966, pp. 26-38.
15. S.A. Gedeon and T.W. Eagar: *Metall. Trans. B*, 1986, vol. 17B, pp. 887-901.